NIPES

Journal of Science and Technology Research

Journal homepage: www.nipesjournals.org.ng

Determining Efficiency of Brushless Permanent Magnet DC Motor Using Magnetic Circuit Simulation

Obi, P.I*[a], Diyoke, G.C[a] and Onwuka, I.K[a]

[a]*Department of Electrical/Electronic Engineering, Michael Okpara University of Agriculture, Umudike, Abia State, Nigeria*
patndyobi@gmail.com

Article Info

***Keywords*:**
Rotor construction, BLPM, Equivalent circuit, pole type, Torque analysis, Efficiency Determination.

Received 03 December 2021
Revised 07 January 2022
Accepted 09 January 2022
Available online 09 March 2022

https://doi.org/10.37933/nipes/4.1.2022.17

https://nipesjournals.org.ng

Abstract

This paper investigates the efficiency of two categories of the four-pole brushless permanent magnet (BLPM) DC motor based on the position of the permanent magnet using magnetic circuit simulation. Finite element analysis (FEA) of the two motors was presented to determine the static and transient characteristics. The performance characteristics of both motors were given in a comparative form. Magnetic properties of the motor such as magnetic flux density, flux lines, air gap flux density were studied. The maximum magnetic flux density and flux lines in motor 1 (pole type 1) were 1.7811 T and $1.5476x10^{-2}$ Wb/m respectively. While that of motor 2 (pole type 2) were 1.8294 T and $1.6925x10^{-2}$ Wb/m respectively. Also, efficiency determination of the motors were performed in which pole type 2 attained maximum efficiency of 93.7% at a speed of 1302 rpm while pole type 1 recorded an efficiency of 82.4% at the same speed. Therefore, there was an efficiency improvement of 11.3% by pole type 2. The maximum power output of pole type 1 and pole type 2 were recorded to be 2.21 kW and 2.47 kW respectively at corresponding speeds of 600 rpm and 780 rpm. Again, it is clear that more power output was given out by motor 2. In order to compare the dynamic behaviors of the two types of the motor during operation; the motor was monitored for a period of 20 ms with time step of 5ms. Both the torque and current characteristics of the pole type 2 recorded an improvement of 47.1% and 50.4% respectively. From the results, the preference to use the motor with pole type 2 has been highlighted. It shows that the motor can offer robust structure with high mechanical strength. It is also suitable for the applications demanding enhanced performance with relatively high speed.

1. Introduction

BLPM DC motors have been widely used because of their attractive features like compactness, low weight, high efficiency, and ease in control [1, 2]. The reliability of brushless DC motor is high since it does not have any brushes to wear out and replace. The stator consists of stacked steel laminations with windings placed in the slots whereas the rotor is made of permanent magnet that can vary from two to twelve pole pairs with alternate north and south poles [3]. It has the capability to provide large volume of torque for wide speed ranges [4]. Electronic commutation technique and permanent magnet rotor cause brushless DC motor to have immediate advantages over brushed DC motor and induction motor in electric vehicle application [5-7].

Permanent magnet motors use permanent magnet in place of electromagnet for excitation. Development in the field of permanent magnet materials and power electronic devices have collectively brought the attention of motor designers to look for efficient and compact permanent magnet motors in various applications. These motors offer many advantages like high efficiency, compactness, higher torque to ampere ratio and high operating speed. These advantages accord the permanent magnet motors the opportunity of emerging as a key technology in many industrial as well as domestic applications [8].

BLPM DC motors are now competing with many other types of motors in industrial applications. However, for low and medium power applications, brushless DC motors are often the main option. Due to its features, these motors are now becoming important for military, aircraft, and automotive applications, and for portable instruments and communications equipment [9, 10]. Nowadays, electric motor manufacturers and researchers are continuously exploring methods for increasing the motor's efficiency which means producing more motor shaft power while using less input power. Motor efficiency improvements will save on energy costs, extend the operation time of battery-powered products and reduce the amount of heat which will increase reliability and can reduce the machine's scheduled maintenance costs [11]. Higher power efficiency also means lower internal power losses and greater power density since power loss defines temperature rise of the motor which is the ultimate performance limitation [12].

The BLPM DC motor construction is similar to the alternating current (AC) permanent magnet synchronous motor with permanent magnets on the rotor and windings on the stator [13, 14]. The energized stator windings create electromagnet poles and permanent magnets create the rotor flux. A rotating field is created on the stator and maintained, by using the appropriate sequence to supply the stator phases. The energized stator phase attracts the rotor. This action of rotor chasing after the electromagnet poles on the stator is the fundamental action used in brushless permanent magnet motors. The permanent-magnet motors technology can be considered as an efficient option due to its high energy generation by permanent magnets which increases the efficiency and also the trade-off which exists between the growth of the manufacturing technology and the decrease in permanent costs [15]. The quick growth of variable-speed drives in the automotive industry based on the hybrid drives is a major industry demand in variable-speed PM drives as well [12, 16]. BLPM DC motor has been considered as a small horsepower control motor [17].

The BLPM DC motor operates based on the rotor position information. According to the rotor position, the phase windings are switched in a sequence to obtain the rotation [4]. The motors are of two types based on the position of permanent magnets on the rotor surface; (1) surface-mounted permanent magnet (SPM) brushless dc motor, (2) interior permanent magnet (IPM) brushless dc motor [8]. In SPM brushless dc motor, the magnets are fixed on the surface of rotor and it will be referred to as pole type 1 in this work. The IPM brushless dc motor will be designated as pole type 2 in this work and it is the type in which the magnets are buried inside the rotor laminations. Figures 1 and 2 show the two poles types adopted in this work respectively.

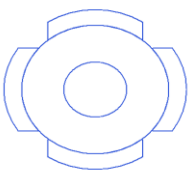

Figure 1: Diagram of Pole Type 1

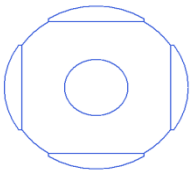

Figure 2: Diagram of Pole Type 2

Basically, electrical machines are electromechanical converters and their behaviours can be described by electromagnetic fields. To solve these fields, magnetic circuit simulation methods have

been recognized as practical and accurate tools. Among these methods, finite element method (FEM) has been proved to be an accurate tool to compute the electromagnetic field distribution and has been extensively used for solving field related problems [18-21]. Hence, it is adopted in this work.

2. Methodology

2.1 Design of the Motor with Magnetic Circuit Software

The three-phase, four-pole brushless PMDC motor was designed and simulated using a magnetic circuit simulation based design software, ANSYS. The results obtained which were given in comparative form were processed with Origin software. The method that was adopted in this work is FEM. FEM is a computer based numerical technique that is used in the calculation of the parameters of electromagnetic devices such as motors, generators, actuators etc. It can be used to calculate the efficiency, flux density, flux linkages, inductance, torque, induced EMF etc., of those devices. In the FEM, the large electromagnetic device is broken down into many small elements [22]. The specifications of the electrical and geometrical parameters of the two motor types used in this work are displayed in Table 1. The computer-aided design is usually the first part of the electric motor development. The machine can be designed with the specified parameters like the materials for the construction of stator and rotor, number of stator slots and number of rotor teeth.

Table 1: Specifications of the brushless PMDC motor

Parameters	Dimensions
Rated Voltage	220 V
Rated Output Power	0.55 kW
Number of Poles	4
Rotor Position	Inner
Given Rated Speed	1500 rpm
Number of Stator Slots	24
Outer Diameter of Stator	120 mm
Inner Diameter of Stator	75 mm
Length of Stator and Rotor	65 mm
Minimum Air Gap	0.5 mm
Inner Diameter of Rotor	26 mm

A single phase equivalent circuit schematic of brushless PMDC motor is shown in Figure 3 [12].

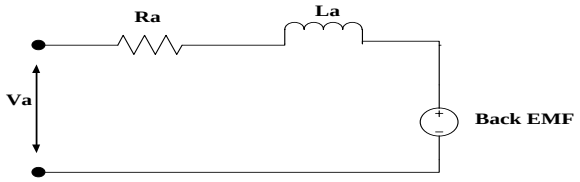

Figure 3: Single Phase Equivalent Circuit of Brushless PMDC Motor

The circuit equations of the three windings in phases are [23]:

$$V_a = R_a i_a + \frac{d\psi_a}{dt} \quad (1)$$

$$V_b = R_b i_b + \frac{d\psi_b}{dt} \quad (2)$$

$$V_c = R_c i_c + \frac{d\psi_c}{dt} \quad (3)$$

where:
Ra, Rb, Rc: Winding Resistances of each phase (Ω),
Va, Vb, Vc: Phase voltages on motor winding (V),
ia, ib, ic: Phase currents (A),
ψa, ψb, ψc: Flux linkages of each phase (Wb).
The flux linkages for each phase are defined as

$$\Psi_a = L_a i_a + L_{ab} i_b + L_{ac} i_c + \Psi_{am} \quad (4)$$

$$\Psi_b = L_b i_b + L_{ba} i_a + L_{bc} i_c + \Psi_{bm} \quad (5)$$

$$\Psi_c = L_c i_c + L_{ca} i_a + L_{cb} i_b + \Psi_{cm} \quad (6)$$

Where
La, Lb, Lc: Self inductances of each phase (H),
Lab, Lac, Lba, Lbc, Lca, Lcb: Mutual inductances between phases (H),
Ψam, ψbm, ψcm: Flux linked with each phase due to the permanent magnet at each phase (Wb).

2.2 Efficiency Determination of Brushless PMDC Motors

The performance of the motor is analyzed via a time-domain simulation. The voltage equation in the time domain is [24]:

$$\begin{bmatrix} v_d \\ v_q \\ v_0 \end{bmatrix} - \begin{bmatrix} e_d \\ e_q \\ e_0 \end{bmatrix} = \begin{bmatrix} R_1 + L_d p & -L_q \omega_e & 0 \\ -L_d \omega_e & R_1 + L_q p & 0 \\ 0 & 0 & R_1 + L_0 p \end{bmatrix} . \begin{bmatrix} i_d \\ i_q \\ i_0 \end{bmatrix} \quad (7)$$

Where R_1, L_d, L_q, and L_0 are armature resistance, d-axis synchronous inductance, q-axis synchronous inductance, and 0-axis inductance, respectively. ω_e is rotor speed in electrical rad/s, and represents for d/dt. The transformations for terminal voltages, induced voltages, and winding currents are given by the following three equations:

$$\begin{vmatrix} v_d \\ v_q \\ v_0 \end{vmatrix} = C^T . \begin{bmatrix} v_a \\ v_b \\ ? \end{bmatrix} : \begin{vmatrix} e_d \\ e_q \\ e_0 \end{vmatrix} = C^T . \begin{bmatrix} e_a \\ e_b \\ ? \end{bmatrix} : \begin{vmatrix} i_a \\ i_b \\ ? \end{vmatrix} = C . \begin{bmatrix} i_d \\ i_q \\ i_0 \end{bmatrix} \quad (8)$$

The transformation matrices for 2-phase, 3-phase, and 4-phases systems, noted as C_2, C_3, and C_4, are as follows:

$$C_2 = \begin{bmatrix} \cos\theta & \sin\theta & 0 \\ \sin\theta & \cos\theta & 0 \end{bmatrix} \tag{9}$$

$$C_3 = \sqrt{\frac{2}{3}} \begin{bmatrix} \cos\theta & \sin\theta & \frac{1}{(\sqrt{2})} \\ \cos(\theta-\alpha) & \sin(\theta-\alpha) & \frac{1}{(\sqrt{2})} \\ \cos(\theta-2\alpha) & \sin(\theta-2\alpha) & \frac{1}{(\sqrt{2})} \end{bmatrix} \tag{10}$$

$$C_4 = \begin{bmatrix} \cos\theta & \sin\theta & 0 \\ \sin\theta & -\cos\theta & 0 \\ -\cos\theta & -\sin\theta & 0 \\ -\sin\theta & \cos\theta & 0 \end{bmatrix} \tag{11}$$

where $\alpha = 2\pi/3$

The input power (electric power) can now be computed from the voltage and current as:

$$P_1 = \frac{1}{t}\int_0^T (v_d i_d + v_q i_q + v_0 i_0)dt \tag{12}$$

The output power (mechanical power) is:

$$P_2 = P_1 - (P_{fw} + P_{cua} + P_t + P_{Fe}) \tag{13}$$

where P_{fw}, P_{Cua}, P_t, and P_{Fe} are frictional and wind loss, armature copper loss, transistor/diode loss, and iron-core loss, respectively.

The output mechanical shaft torque T_2 is:

$$T_2 = \frac{P_2}{\omega} \tag{14}$$

where ω is the rotor speed in mechanical rad/s.

The efficiency is computed by:

$$efficiency = \frac{P_2}{P_1} * 100\% \tag{15}$$

3. Results and Discussion

It is important to predict accurately the steady state and dynamic performances of the BLPM DC motors in order to avoid the design misjudgment that can prove costly once the motors are manufactured. The results will assist in identifying the motor type that is more efficient and reliable. The performance characteristics of both motors which include compactness, high efficiency, ease in control, high reliability and large torque are given in a comparative form.

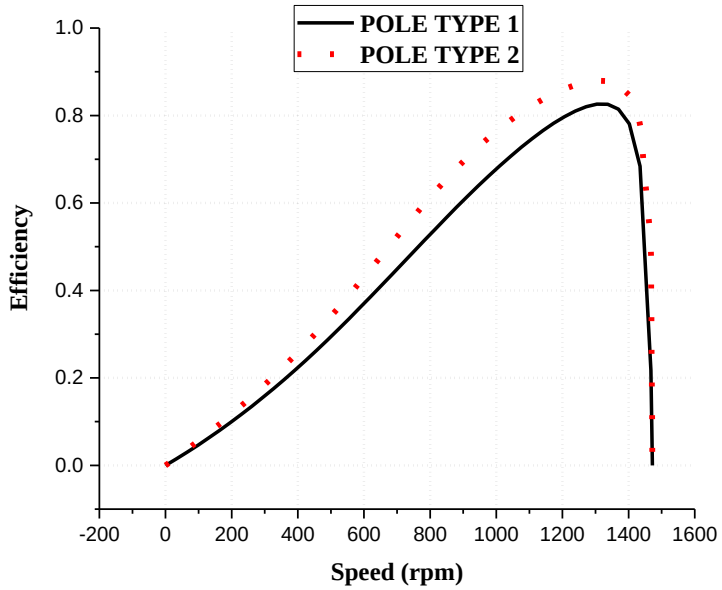

Figure 4: Efficiency and Speed

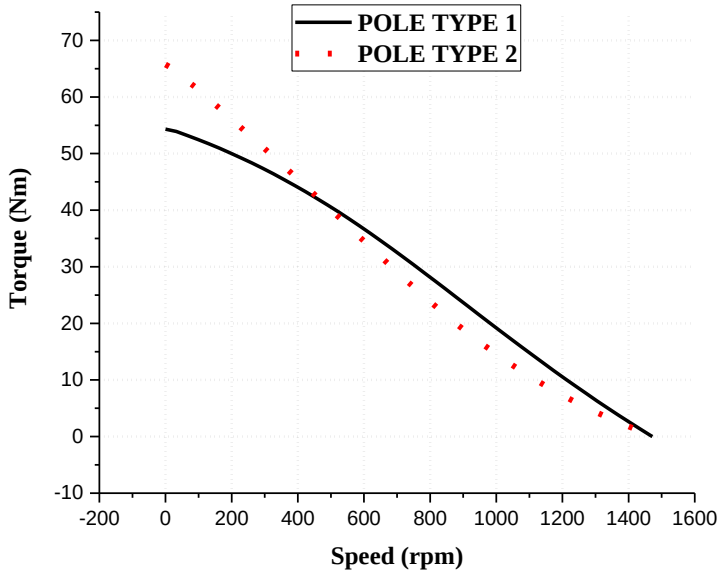

Figure 5: Torque and Speed

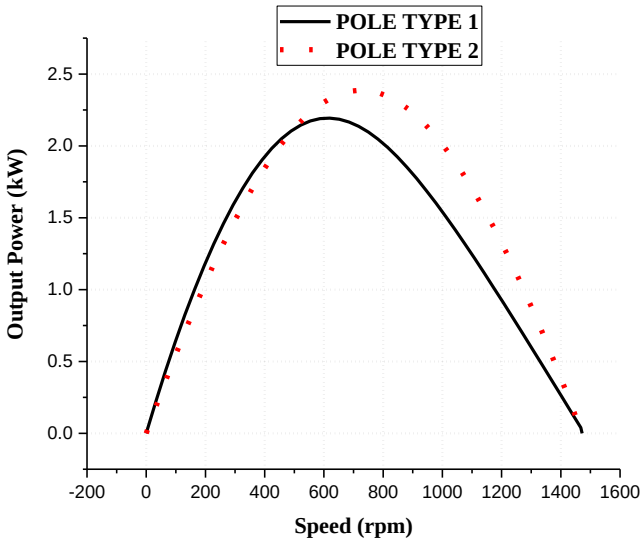

Figure 6: Output Power and Speed

Figure 4 shows the efficiency and speed relationship of both motor types. When both motors' rotors start rotating, efficiency and speed increased proportionally until they attained their peak efficiencies of 82.4% and 93.7% respectively at a corresponding speed of 1302 rpm. Therefore, there was efficiency improvement of 11.3% even at the same speed.

Figure 5 compares the output torque against speed. At zero speed, the torques of both motors were very high (54.8 Nm and 67 Nm respectively). As the speed increased, the torques decreased until it becomes zero at speeds of 1480 rpm and 1400 rpm respectively.

Figure 6 shows the output power versus the speed. It is obvious that, when the rotors of motor 1 and motor 2 were stationary, no output power or speed was recorded. But when the rotors began to rotate, both quantities increased linearly. They reached maximum power output of 2.21 kW and 2.47 kW respectively at corresponding speeds of 600 rpm and 780 rpm. Again, it is clear that more power output is given out by motor 2.

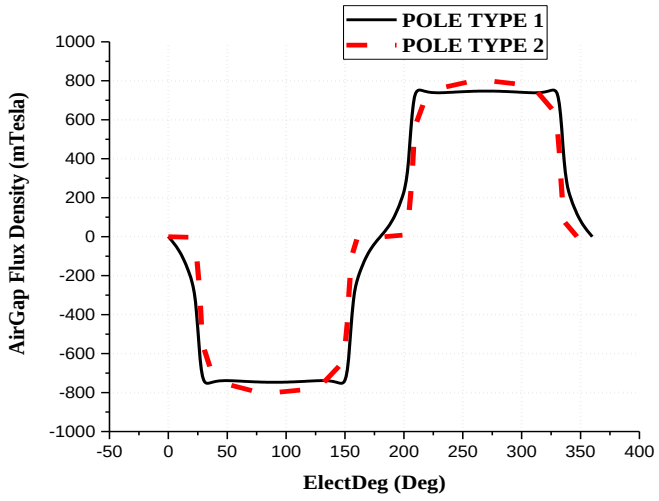

Figure 7: Air gap Flux Density and Electric Degrees

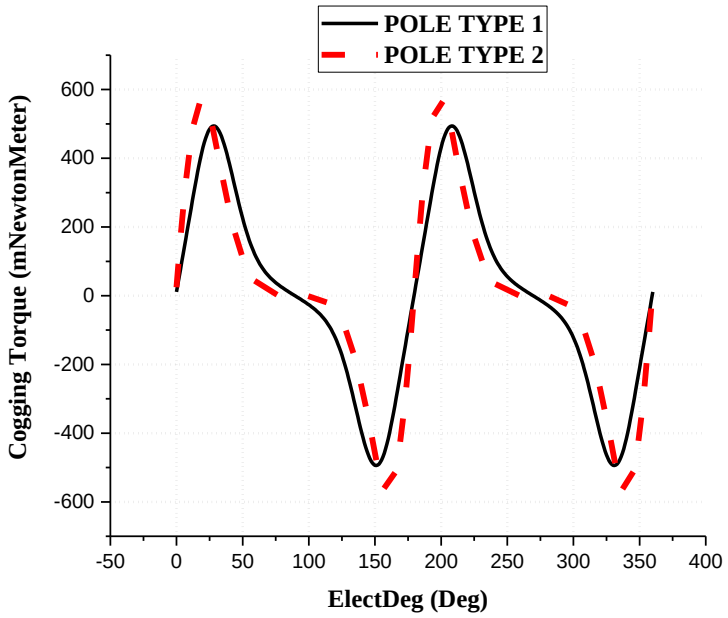

Figure 8: Cogging Torque and Electric Degrees

Figures 7 and 8 show the variation of flux density and cogging torque with electric degrees respectively. Motor 2 recorded higher flux density and cogging torque of 800 mT and 590 mNm respectively than that of motor 1 with 660 mT and 482 mNm respectively.

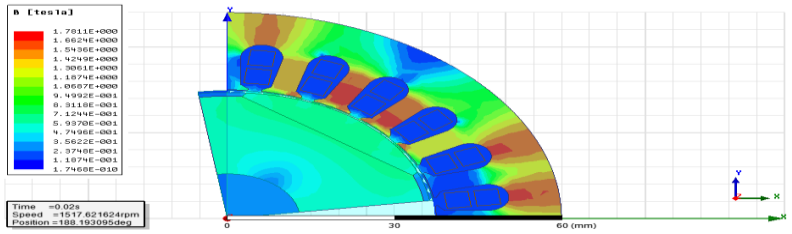

Figure 9: Magnetic Flux Density of Pole Type 1

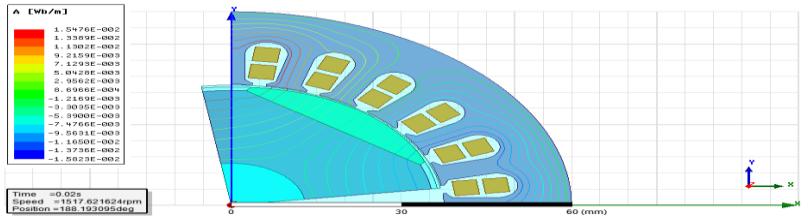

Figure 10: Magnetic Flux Lines of Pole Type 1

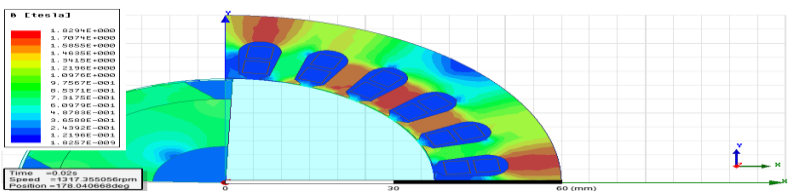

Figure 11: Magnetic Flux Density of Pole Type 2

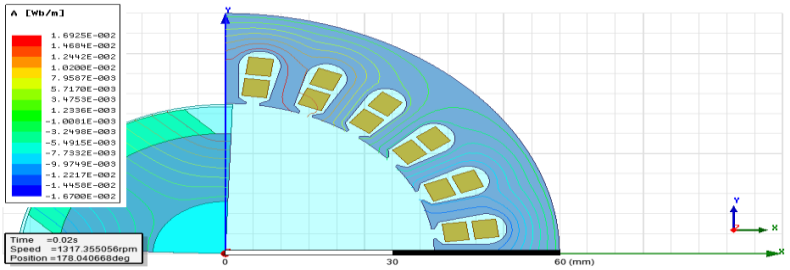

Figure 12: Magnetic Flux Lines of Pole Type 2

In order to compare the dynamic behaviors of the two models during the operation, the motors were monitored for 20 ms. Speed, current and electromagnetic torque have been observed as shown in Figures 9-11. The dynamic parameters of the models are: initial angular velocity = 1500 rpm, moment of inertia = 0.00149257 kgm^2, damping coefficient = 0.0018845 Nms/rad, time step = 5 ms, stop time = 20 ms.

Figures 9 and 10 are the flux density and flux lines of pole type 1. The range of magnetic flux density in motor 1 is between 1.7468x10^{-10} T and 1.7811 T. While the range of flux lines is between -9.5631x10^{-3} Wb/m and 1.5476x10^{-2} Wb/m. At a stop time of 0.02s, the speed and position of the rotor of pole type 1 were 1517.62 rpm and 188.19 deg respectively.

The range of magnetic flux density as observed in motor 2 is 1.8257x10^{-9} T – 1.8294 T as seen in Figure 11. Figure 12 shows the flux lines in the motor. The maximum and minimum magnetic flux lines are 1.6925x10^{-2} Wb/m and -9.9749x10^{-3} Wb/m respectively. The speed and position of the rotor of motor 2 at the end of the simulation was found to be 1317.36 rpm and 178.04 deg respectively.

The difference in the speed and rotor position of the two types of motor is because of the position of the permanent magnet on the pole of the rotor of each of the motors.

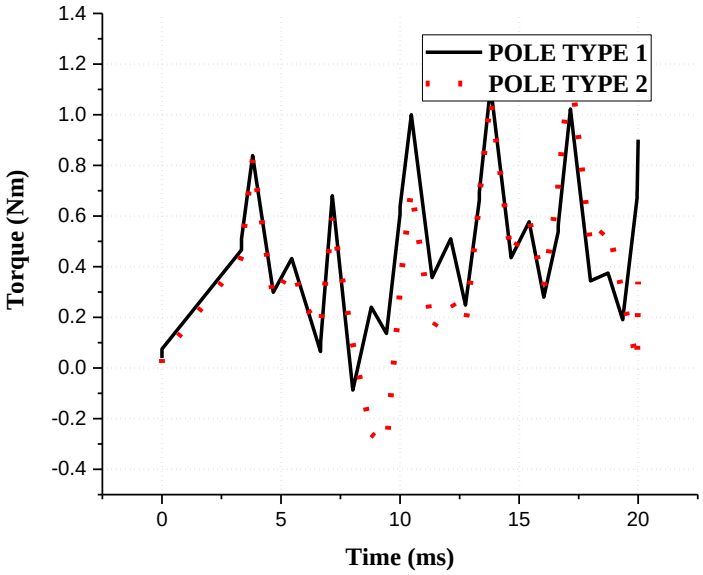

Figure 13: Torque and Time

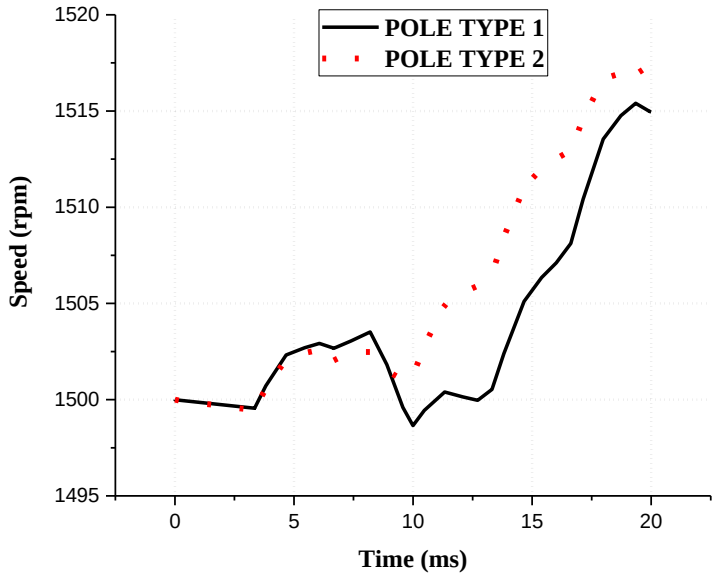

Figure 14: Speed and Time

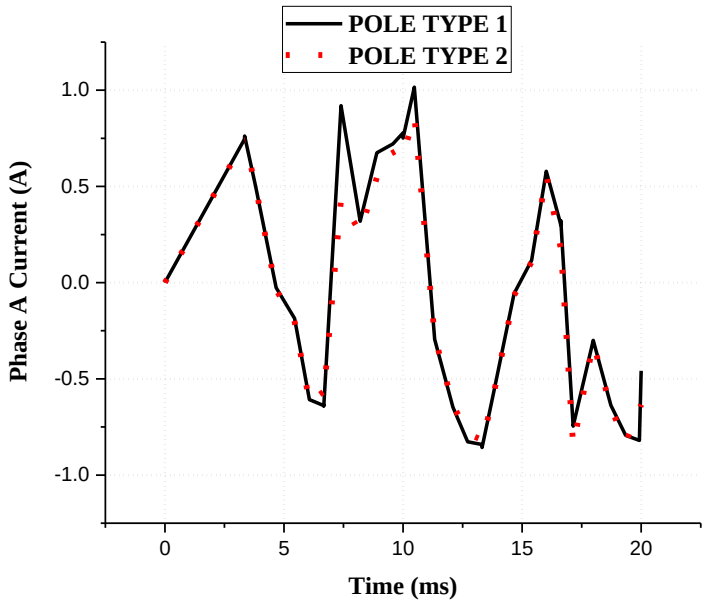

Figure 15: Phase A Current with Time

From Figure 13, the peak torque observed in pole type 1 is 1 Nm while it is 0.68 Nm in pole type 2 with percentage variation of 47.1%.

There was an improvement in the speed of pole type 2 when compared with pole type 2 as recorded in Figure 14. At the stop time of 0.02 s, the speed of pole types 1 and 2 were 1515 rpm and 1517.5 rpm respectively.

Current waveforms for pole type 1 and pole type 2 are given in Figure 15. When the waveforms were examined, the maximum current is 1.21 A for pole type 1 and 0.6 A for pole type 2. This shows that the phase current for pole type 1 has high transients, whereas these transients were reduced in pole type 2 with an improvement of 50.4%.

4. Conclusion

The comprehensive design of two categories of 550 W, 1500 rpm , four-pole brushless permanent magnet (BLPM) DC motor based on the position of the permanent magnet were performed. Finite element analysis (FEA) of the two motors was presented to determine the static and transient characteristics**.** The dimensions of each part of the motor were calculated along with performance estimation. The performance characteristics of both motors were given in a comparative form. Some of magnetic properties of the motor like magnetic flux density, flux lines, air gap flux density were studied.

The range of magnetic flux density in motor 1 was between 1.7468×10^{-10} T and 1.7811 T. While the range of flux lines was between -9.5631×10^{-3} Wb/m and 1.5476×10^{-2} Wb/m. At a stop time of 0.02s, the speed and position of the rotor of pole type 1 were 1517.62 rpm and 188.19 deg respectively. While in pole type 2, the range of magnetic flux density was 1.8257×10^{-9} T – 1.8294 T. The maximum and minimum magnetic flux lines of the motor were 1.6925×10^{-2} Wb/m and -9.9749×10^{-3} Wb/m respectively. The speed and position of the rotor of motor 2 at the end of the simulation was found to be 1317.36 rpm and 178.04 deg respectively. The difference in the speed and rotor position of the two types of motor is because of the position of the permanent magnet on the pole of the rotor of each of the motors.

Also, efficiency determination of the motors were performed in which pole type 2 attained maximum efficiency of 93.7% at a speed of 1302 rpm while pole type 1 recorded an efficiency of 82.4% at the same speed. Therefore, there was an efficiency improvement of 11.3% by pole type 2. The maximum power output of pole type 1 and pole type 2 were recorded to be 2.21 kW and 2.47 kW respectively at corresponding speeds of 600 rpm and 780 rpm. Again, it is clear that more power output was given out by motor 2.

In order to compare the dynamic behaviors of the two types of the motor during operation; the motors were monitored for a period of 20 ms with time step, moment of inertia and damping coefficient of 5ms, 0.00149257 kgm^2 and 0.0018845 Nms/rad respectively. Speed, current and electromagnetic torque were monitored. Both the torque and current characteristics of the pole type 2 recorded an improvement of 47.1% and 50.4% respectively. From the results, the preference to use the motor with pole type 2 has been highlighted. It shows that the motor can offer robust structure with high mechanical strength. It is also suitable for the applications demanding enhanced performance with relatively high speed.

References

[1] L. Parsa (2005). On Advantages of Multiphase Machines. 31st Annual Conference of Industrial Electronics 2005, IECON, Raleigh, NC, USA, 6-10 November, 2005, pp. 1574-1579.
[2] V. Sandeep and S. Shastri (2019). Analysis and Design of PMBL DC motor for Three Wheeler Electric Vehicle Application. E3S Web of Conferences, Vol. 87(6), pp. 1-7.
[3] K. S. Shinoy, B. Sebastian, and M. N. Namboodiripad (2016). Design of 100kW Brushless DC Motor for Advanced Actuation System using Comsol. Proceedings of the 2016 COMSOL Conference in Bangalore, pp. 1-5.
[4] E. Elakkia, S. Anita, R. Girish and S. Saikiran (2015). Design and Modelling of BLDC Motor for Automotive Applications. National Level Technical Conference, Special Issue, Vol. 1(1), pp. 42-48.

[5] M. P. Jainesh, V. H. Hitesh and R. Mulav (2014). Simulation and Analysis of Brushless DC Motor Based on Sinusoidal PWM Control. Vol. 2(3), pp. 1236-1238.
[6] A. Tashakori, M. Ektesabi, and N. Hosseinzadeh (2011). Characteristic of Suitable Drive Train for Electric Vehicle. 2011 International Conference on Instrumentation, Measurement, Circuits and Systems (ICIMCS 2011), Vol. 2, Hong Kong, China, 12-13 December, 2011, pp. 20-29.
[7] T. Mathew and A. Caroline (2013). Modeling and Closed Loop Control of BLDC Motor Using a Single Current Sensor. International Journal of Advanced Research in Electrical Electronics and Instrumentation Engineering, vol. 2(6), pp. 978-988.
[8] N. P. Amit and H. P. Tejas (2018). Design and FE Analysis of Interior Permanent Magnet (IPM) Brushless DC Motor. International Journal of Pure and Applied Mathematics, Vol. 118(17), pp. 915-924.
[9] A. K. Mishra, M. K. Roy, V. S. Mohalkar and R. Mishra (2012). BLDC Technology and its Application in Weapon System Launching Platform. International Journal of Engineering, Science and Technology Vol. 4(1), pp. 8-15.
[10] K. J. Bathe (2016). Finte Element Procedures 2nd Edition https://web.mit.edu./kjb Accessed 26 October, 2021.
[11] W. Brown (2002). Brushless DC Motor Control Made Easy. Microchip Technology Incorporated.
[12] N. B. Othman (2012). Design and Evaluation of High Power Density Brushless DC Permanent Magnet Machines. PhD Thesis, University of Nottingham.
[13] J. Faiz and B. M. Ebrahimi (2006). Mixed Fault Diagnosis in Three-Phase Squirrel-Cage Induction Motor using Analysis of Air-Gap Magnetic Field. Progress in Electromagnetics Research, PIER 64, pp. 239-255.
[14] H. Moradi, E. Afjei and F. Faghihi (2009). FEM Analysis for a Novel Configuration of Brushless DC Motor without Permanent Magnet. Progress in Electromagnetics Research, PIER 98, pp. 407-423.
[15] T. J. E. Miller (2001). Electronic Control of Switched Reluctance Machines. Newnes Engineering Series 1st Edtion. https://www.amazon.com/Electronic-Switched-Reluctance-Machines-Engineering/dp/0750650737 Accessed 26 October, 2021.
[16] T. J. E. Miller (1993). Brushless Permanent-Magnet and Reluctance Motor Drives. Oxford Cleredon Press. https://www.worldcat.org/title/brushless Accessed 26 October, 2021.
[17] E. Idoko, F. T. Ikule and P. I. Udenze (2019). Performance of Brushless Permanent Magnet DC Motor with Different Rotor Positions Using ANSYS. International Journal of Advanced Engineering Research and Technology (IJAERT), Vol. 7(3), pp. 2348-8190.
[18] C. Johnson (2009). Numerical Solution of Partial Differential Equations by Finite Element Method. 2nd Edition. Cambridge University press, Ney York, p. 278.
[19] S. S. Rao (2011). The Finite Element Method in Engineering. 5th Edition https://www.sciencedirect.com Accessed 26 October, 2021.
[20] K. H. Huebner, D. L. Dewhirst, D. E. Smith and T. G. Byrom (2001). The Finite Element Method for Engineers" 4th Edition. https://www.willy.com/en-us/The+Finite+Element+Method+for+Engineers Accessed 22 October, 2021.
[21] N. P. Hla (2004). Numerical Analysis of a Brushless Permanent Magnet DC Motor using Coupled Systems. Thesis, Electrical and Computer Engineering National University of Singapore.
[22] A. Arkkio (1990). Finite Element Analysis of Cage Induction Motors Fed By Static Frequency Converters. IEEE Transactions on Magnetics, vol. 26, pp. 551-554.
[23] S. E. Lyshevski (2008). Electromechanical System and Devices. CRC Press, Boca Raton, London, p.565.
[24] ANSYS Electromagnetics (2018), ANSYS Inc.